nature immunology

Dominant-activating germline mutations in the gene encoding the PI(3)K catalytic subunit p110δ result in T cell senescence and human immunodeficiency

Carrie L Lucas[1,15], Hye Sun Kuehn[2,15], Fang Zhao[3,4,15], Julie E Niemela[2], Elissa K Deenick[5,6], Umaimainthan Palendira[5,6], Danielle T Avery[5], Leen Moens[5], Jennifer L Cannons[3], Matthew Biancalana[1], Jennifer Stoddard[2], Weiming Ouyang[7], David M Frucht[7], V Koneti Rao[1], T Prescott Atkinson[8], Anahita Agharahimi[9,10], Ashleigh A Hussey[9], Les R Folio[11], Kenneth N Olivier[9], Thomas A Fleisher[2], Stefania Pittaluga[12], Steven M Holland[9], Jeffrey I Cohen[13], Joao B Oliveira[14], Stuart G Tangye[5,6], Pamela L Schwartzberg[3], Michael J Lenardo[1] & Gulbu Uzel[9]

The p110δ subunit of phosphatidylinositol-3-OH kinase (PI(3)K) is selectively expressed in leukocytes and is critical for lymphocyte biology. Here we report fourteen patients from seven families who were heterozygous for three different germline, gain-of-function mutations in *PIK3CD* (which encodes p110δ). These patients presented with sinopulmonary infections, lymphadenopathy, nodular lymphoid hyperplasia and viremia due to cytomegalovirus (CMV) and/or Epstein-Barr virus (EBV). Strikingly, they had a substantial deficiency in naive T cells but an over-representation of senescent effector T cells. *In vitro*, T cells from patients exhibited increased phosphorylation of the kinase Akt and hyperactivation of the metabolic checkpoint kinase mTOR, enhanced glucose uptake and terminal effector differentiation. Notably, treatment with rapamycin to inhibit mTOR activity *in vivo* partially restored the abundance of naive T cells, largely 'rescued' the *in vitro* T cell defects and improved the clinical course.

The phosphatidylinositol-3-OH kinase (PI(3)K) pathway has crucial roles throughout eukaryotic biology. In mammals, there are three classes of PI(3)K that are distinct in their mechanisms of regulation, substrate specificity and structure[1]. All classes of PI(3)K phosphorylate the inositol ring of phosphatidylinositol lipids in membranes, and several of these enzymes can also phosphorylate protein substrates at serine and/or threonine residues[2]. Class I PI(3)K molecules have the largest role in cells of the immune system and are composed of a catalytic p110 subunit and a regulatory p85 subunit that governs the stability, membrane localization and activity of p110. Among the class I PI(3)K molecules, only p110δ (Online Mendelian Inheritance in Man catalog accession code, 602839) is restricted to leukocytes[3,4] and has specialized functions in adaptive immunity. Activation of p110δ requires the ligation of cell-surface receptors linked to tyrosine kinase activity, which leads to recruitment of the PI(3)K complex to pYxxM motifs (where 'pY' indicates phosphorylated tyrosine and 'x' indicates any amino acid) via two Src-homology 2 (SH2) domains in the regulatory p85 subunit[5]. Binding of p85 to phosphorylated tyrosine relieves its inhibition of p110 and enables p110-mediated phosphorylation of phosphatidylinositol-(4,5)-bisphosphate (PtdIns(4,5)P_2) to generate phosphatidylinositol-(3,4,5)-trisphosphate (PtdIns(3,4,5)P_3), which initiates the recruitment of pleckstrin homology domain–containing signaling proteins to the plasma membrane. Negative regulators of PI(3)K include the phosphatases PTEN and SHIP, which convert PtdIns(3,4,5)P_3 into PtdIns(4,5)P_2 and PtdIns(3,4)P_2, respectively. Despite a vast literature on PI(3)K, the basic question of how p110δ activity modulates human immunity remains unanswered.

T cell function is heavily dependent on the regulation of cellular metabolism to control proliferative capacity, effector function and

[1]Molecular Development of the Immune System Section, Laboratory of Immunology, National Institute of Allergy and Infectious Diseases, National Institutes of Health, Bethesda, Maryland, USA. [2]Department of Laboratory Medicine, Clinical Center, National Institutes of Health, Bethesda, Maryland, USA. [3]Cell Signaling Section, Genetic Disease Research Branch, National Human Genome Research Institute, National Institutes of Health, Bethesda, Maryland, USA. [4]Pritzker School of Medicine, The University of Chicago, Chicago, Illinois, USA. [5]Immunology and Immunodeficiency Group, Immunology Program, Garvan Institute of Medical Research, Sydney, Australia. [6]St. Vincent's Clinical School Faculty of Medicine, University of New South Wales, Sydney, Australia. [7]Laboratory of Cell Biology, Division of Monoclonal Antibodies, Office of Biotechnology Products, Center for Drug Evaluation and Research, United States Food and Drug Administration, Bethesda, Maryland, USA. [8]Division of Allergy and Immunology, Department of Pediatrics, University of Alabama at Birmingham, Birmingham, Alabama, USA. [9]Laboratory of Clinical Infectious Diseases, National Institute of Allergy and Infectious Diseases, National Institutes of Health, Bethesda, Maryland, USA. [10]Laboratory of Clinical Infectious Diseases, Clinical Research Directorate–Clinical Monitoring Research Program, Science Applications International Corporation–Frederick, Frederick National Laboratory for Clinical Research, Frederick, Maryland, USA. [11]Radiology and Imaging and Sciences, Clinical Center, National Institutes of Health, Bethesda, Maryland, USA. [12]Laboratory of Pathology, National Cancer Institute, National Institutes of Health, Bethesda, Maryland, USA. [13]Laboratory of Infectious Diseases, National Institute of Allergy and Infectious Diseases, National Institutes of Health, Bethesda, Maryland, USA. [14]Instituto de Medicina Integral Prof. Fernando Figueira, Recife-Pernambuco, Brazil. [15]These authors contributed equally to this work. Correspondence should be addressed to G.U. (guzel@niaid.nih.gov)

Received 20 September; accepted 21 October; published online 28 October 2013; doi:10.1038/ni.2771.

the generation of memory[6]. The metabolic checkpoint kinase mTOR (mechanistic target of rapamycin), which is activated by PI(3)K, has a prominent role in promoting dynamic changes in T cell metabolism[7,8]. PI(3)K has been described as activating mTOR complex 2 (composed of mTOR, Rictor and GβL) by promoting its association with ribosomes[9]. Moreover, the PtdIns(3,4,5)P_3 generated by PI(3)K recruits both the kinase PDK1 and the kinase Akt (PKB) and thereby enables full activation of Akt through phosphorylation at Thr308 (by PDK1) and Ser473 (by mTOR complex 2)[10,11]. In its active form, Akt activates mTOR complex 1 (mTORC1; composed of mTOR, Raptor and GβL), which leads to phosphorylation of the translation-initiation inhibitor 4E-BP1 and the kinase p70S6K to promote protein translation[12]. Phosphorylation of 4E-BP1 results in its release from the translation-initiation factor eIF4E and promotes cap-dependent translation, whereas phosphorylation of p70S6K activates the ribosomal protein S6 to enhance the translation of ribosomal proteins and elongation factors. One of the proteins whose expression is increased by mTORC1 activity is the transcription factor HIF-1α, a key regulator of glycolysis[13]. Thus, in cells with high PI(3)K-Akt-mTOR activity, a metabolic shift toward glycolysis would be expected, and indeed this occurs after the differentiation of naive T cells into effector T cells[14]. In addition to enhancing HIF-1α expression, mTORC1 activity promotes the translation and stability of the tumor suppressor p53 and has been linked to the role of p53 in inducing cellular senescence[15]. However, it is unknown how constitutive activation of the Akt-mTOR pathway affects T cell function and immunity in humans.

When a naive T cell encounters antigen, a differentiation process ensues that generates both short-lived effector cells that respond to the acute phase of infection as well as long-lived memory cells that ensure a rapid and vigorous immune response if the same antigen is reencountered. For $CD8^+$ T cells, the Akt-mTOR pathway has been highlighted as a critical mediator of differentiation into short-lived effector cells versus memory precursor effector cells[16]. When Akt-mTOR signaling is sustained, a transcriptional program that promotes effector function drives cells toward differentiation into terminal effector cells at the expense of memory formation[17,18]. Mounting evidence suggests that effector cells must 'reset' their metabolic activity to become memory cells. Naive $CD8^+$ T cells use fatty-acid oxidation and mitochondrial respiration to meet their relatively low energy demands; however, after the activation of naive cells, a switch to lipid synthesis and glycolysis is necessary to rapidly provide the cell with sufficient energy to carry out effector functions. To survive and contribute to the memory pool, effector $CD8^+$ T cells must revert back to the catabolic processes of fatty-acid oxidation and mitochondrial respiration[12]. The Akt-mTOR pathway is a central mediator of that switch, as it promotes glucose uptake, glycolysis and lipid synthesis, all processes crucial for the differentiation of $CD8^+$ T cells[19]. Therefore, it is of great interest to determine how alterations in these metabolic pathways in cells of the immune system can affect T cell differentiation and human health. Here we describe a group of patients with combined immunodeficiency and lymphoproliferative disease who share gain-of-function mutations in *PIK3CD* (which encodes p110δ). Those mutations resulted in hyperactivation of mTOR signaling and skewed the differentiation of $CD8^+$ T cells to short-lived effector cells with severely impaired development of functional memory T cells and B cells.

RESULTS

Immunodeficiency, memory abnormalities and effector skewing

We evaluated nine patients from seven unrelated families of different ethnic and racial backgrounds who presented with childhood onset sinopulmonary infections, lymphoproliferation (**Supplementary Fig. 1a**,**b**), chronic viremia due to Epstein-Barr virus (EBV) and/or cytomegalovirus (CMV), and distinctive nodular lymphoid ($CD3^+$ and $CD20^+$) hyperplasia of mucosal surfaces (**Table 1**, **Fig. 1a**, **Supplementary Table 1**

Table 1 Patient characteristics

	Kinase domain			Helical domain					C2 domain
	A.1	**B.III.1**	**C.1**	**D.I.1**	**D.II.1**	**D.II.2**	**E.1**	**F.II.1**	**G.1**
Age, sex	12, M	14, F	15 (†), F	40, M	15, M	12, F	7, F	17, F	12, F
EBV viremia	✓	✓	✓	✓	✓	✓	✓	✓	✓
CMV	✓	Naive	ND	✓	✓	✓	✓	Naive	Naive
Sinopulmonary bacterial infections	✓	✓	✓	✓	✓	✓	✓	✓	✓
Lymphoma diagnosis	No	No*	EBV^+ diffuse B cell lymphoma	No	No	No	No	EBV^+ nodular sclerosis Hodgkin	No
Lymphadenopathy	✓	✓	✓	No	✓	No	✓	✓	✓
Mucosal lymphoid aggregates	✓	ND	ND	✓	✓	✓	✓	ND	✓
T & B lymphocyte subsets	$CD4^+$ ↓	$CD4^+$ ↓	$CD4^+$ ↓	$CD4^+$ ↓	$CD4^+$ ↓	$CD4^+$ ↓	$CD4^+$ ↓	$CD4^+$ nl	$CD4^+$ ↓
	$CD4^+$ naive ↓	$CD4^+$ naive ↓	$CD4^+$ naive ↓	$CD4^+$ naive ↓	$CD4^+$ naive ↓	$CD4^+$ naive ↓	$CD4^+$ naive ↓	$CD4^+$ naive nl	$CD4^+$ naive ↓
	$CD8^+$ CM, EM ↑	$CD8^+$ effector ↑	$CD8^+$ effector ↑	$CD8^+$ EM ↑	$CD8^+$ CM & EM ↑	$CD8^+$ CM & EM nl	$CD8^+$ EM ↑	$CD8^+$ CM, EM ↑	$CD8^+$ EM ↑
	$CD5^+CD20^+$ ↑	$CD5^+CD20^+$ ↑	$CD5^+CD20^+$ ↑	$CD5^+CD20^+$ ↑	$CD5^+CD20^+$ ↑	$CD5^+CD20^+$ ↑	$CD5^+CD20^+$ ↑	$CD5^+CD20^+$ ↑	$CD5^+CD20^+$ ↑
	Bmem switch ↓	Bmem switch ↓	ND	Bmem switch nl	Bmem switch ↓	Bmem switch nl	Bmem switch ↓	Bmem switch ↓	Bmem switch ↓
T_{reg} cells**	nl	nl	nl	ND	ND	ND	↑	nl	↓
$CD3^+CD8^+CD57^+$ cells	44%	ND	42%	ND	35%	ND	ND	ND	41%
NK cells	NK nl	NK nl	NK nl	NK ↓	NK ↓	NK nl	NK ↑	NK nl	NK nl
	NKT nl	NKT nl	NKT nl	NKT ↑	NKT ↓	NKT nl	NKT ↑	NKT nl	NKT nl
Immunoglobulins	IgG↓, IgA↓	IgG nl, IgA nl	IgG↓, IgA↓	IgG↑, IgA nl	IgG↓, IgA↓	IgG↑, IgA↓	nl	IgG nl IgA↓	IgG↓, IgA↓
	IgM↑	IgM↑	IgM↓	IgM nl	IgM nl	IgM nl		IgM nl	IgM↑

Infections, lymphoma, lymphoproliferation and immunological phenotypes of patients. M, male; F, female; †, deceased; ✓, present; ↓, decreased abundance; ↑, increased abundance; ND, not determined; nl, normal; Bmem switch, class-switched memory B cells; NK, natural killer. *Family history of B cell lymphoma; **other helper T cell subsets detected at normal frequencies.

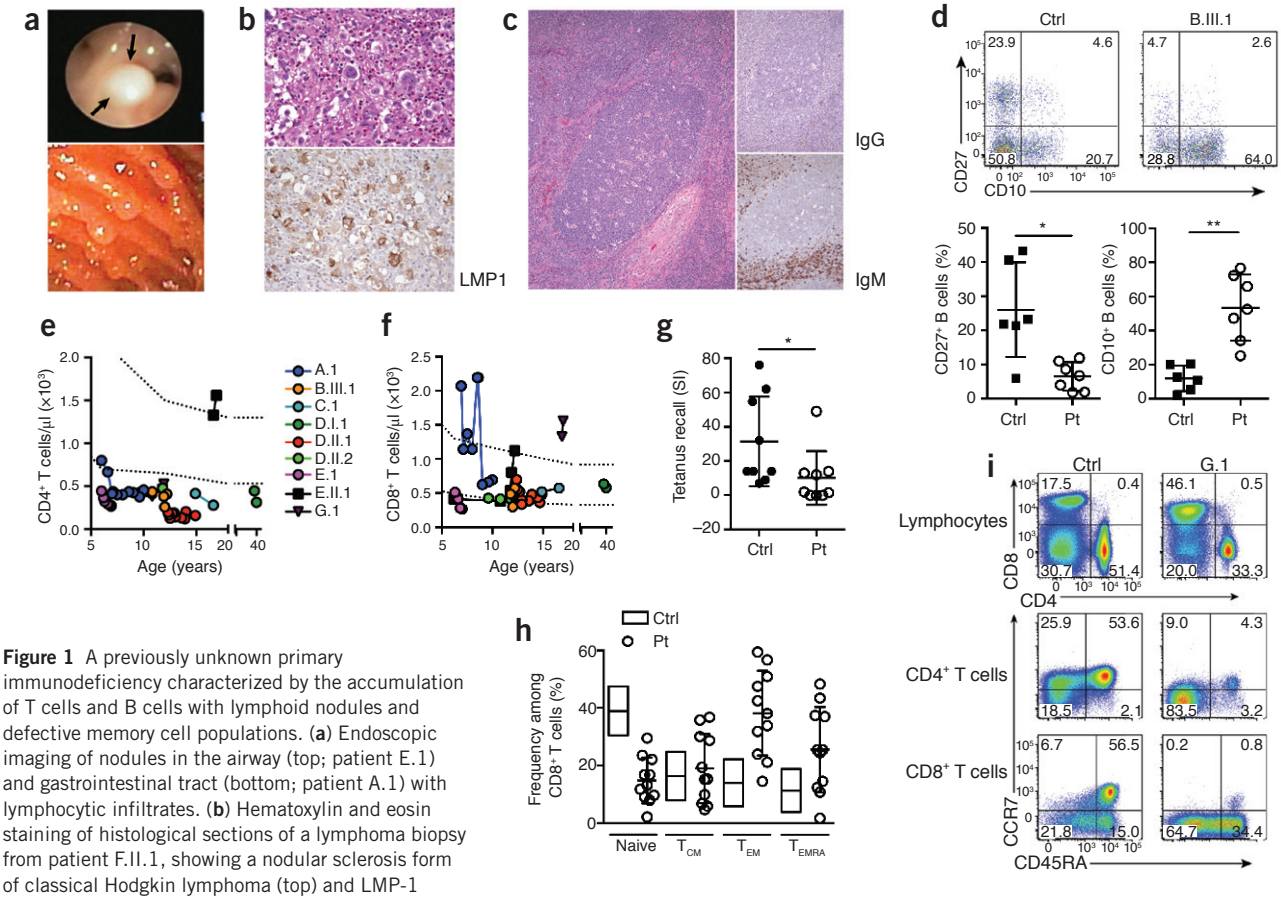

Figure 1 A previously unknown primary immunodeficiency characterized by the accumulation of T cells and B cells with lymphoid nodules and defective memory cell populations. (**a**) Endoscopic imaging of nodules in the airway (top; patient E.1) and gastrointestinal tract (bottom; patient A.1) with lymphocytic infiltrates. (**b**) Hematoxylin and eosin staining of histological sections of a lymphoma biopsy from patient F.II.1, showing a nodular sclerosis form of classical Hodgkin lymphoma (top) and LMP-1 staining of EBV latent membrane antigen (brown (3,3′-diaminobenzidine); bottom). (**c**) Hematoxylin and eosin staining (left) and immunoperoxidase staining for IgG (top right) and IgM (bottom right) on histological sections of lymph nodes from patient G.1. (**d**) Flow cytometry (top) of transitional cells ($CD27^-CD10^+$; bottom right quadrant), naive cells ($CD27^-CD10^-$; bottom left quadrant) and memory cells ($CD27^+CD10^-$; top left quadrant) among B cells from a healthy control subject (Ctrl) or patient B.III.1. Numbers in quadrants indicate percent cells in each throughout. Below, cumulative data for memory B cells (left) and transitional B cells (right) detected as above. Each symbol represents an individual healthy control subject (Ctrl; $n = 6$) or patient (Pt; $n = 7$); small horizontal lines indicate the mean (± s.d.). $^*P = 0.004$ and $^{**}P = 0.0005$ (two-tailed, unpaired *t*-test). (**e**,**f**) Quantification of $CD4^+$ T cells (**e**) and $CD8^+$ T cells (**f**) in peripheral blood from patients (key; $n = 9$) as a function of age. (**g**) Thymidine-incorporation assay of proliferation in response to the tetanus recall antigen, presented as the stimulation index (SI; value obtained with antigen / value obtained without antigen). Each symbol represents an individual healthy control subject ($n = 9$) or patient ($n = 9$); small horizontal lines indicate the mean (± s.d.). $^*P = 0.01$ (Mann-Whitney test). (**h**) Frequency of naive T cells ($CD45RA^+CD62L^+$), central memory T cells (T_{CM}; $CD45RA^-CD62L^+$), T_{EM} cells ($CD45RA^-CD62L^-$) and T_{EMRA} cells ($CD45RA^+CD62L^-$) among $CD8^+$ T cells in all living patients, as well as the clinical normal range (boxes) derived from healthy adult control subjects ($n = 50$). Each symbol represents an individual patient ($n = 11$); small horizontal lines indicate the mean (± s.d.). (**i**) Flow cytometry of PBMCs from a healthy control subject and patient G.1, stained for CD8 versus CD4 (gated on lymphocytes; top) or for CCR7 versus CD45RA, gated on $CD4^+$ lymphocytes (middle) or $CD8^+$ lymphocytes (bottom), identifying naive T cells ($CD45RA^+CCR7^+$; top right quadrant), central memory T cells ($CD45RA^-CCR7^+$; top left quadrant), T_{EM} cells ($CD45RA^-CCR7^-$; bottom left quadrant) and T_{EMRA} cells ($CD45RA^+CCR7^-$; bottom right quadrant) (additional data, **Supplementary Fig. 1d**). Data are representative of six experiments with one patient in each (**a**), thirteen experiments with samples from six total patients (**c**), or five independent experiments (**d**,**i**) or are from one experiment (**b**), one experiment with two to ten independent measurements for each patient (**e**,**f**), eleven experiments with one patient in each (**h**) or nine independent experiments with one patient in each (**g**).

and **Supplementary Fig. 1**). We also observed autoimmune cytopenia in several patients (**Supplementary Table 1**). Of relevance, EBV-driven B cell lymphoma occurred in two index patients (C.1 and F.II.1), one of whom (F.II.1) was diagnosed with an EBV^+ nodular sclerosis form of classical Hodgkin lymphoma (**Fig. 1b**), which is characteristically observed in immunodeficient patients[20]. Additionally, a 12-year-old patient (B.III.1) with extensive nonmalignant lymphoproliferation represents the third generation of a family in which two other members had EBV-associated lymphomas (in support of an autosomal-dominant inheritance pattern). Although lymph node architecture was preserved, B cell follicles had prominent germinal centers with no mantle zones and no detectable staining of immunoglobulin G (IgG) (**Fig. 1c**). Notably, the peripheral blood B cell compartment lacked memory $CD27^+$ B cells and showed enrichment for immature transitional $CD10^+$ B cells (**Fig. 1d**). We observed progressive $CD4^+$ T cell lymphopenia (**Fig. 1e**) with normal to high $CD8^+$ T cell counts (**Fig. 1f** and **Table 1**). The responses of T cells from patients to *in vitro* mitogen stimulation were poor (**Supplementary Fig. 1c**), as were their responses to recall challenge with tetanus (**Fig. 1g**). Notably, these patients had a reversed ratio of $CD4^+$ T cells to $CD8^+$ T cells and a much lower abundance of $CD45RA^+CCR7^+$ naive T cells, with a correspondingly greater abundance of $CD45RA^-CCR7^-$ effector memory T cells (T_{EM} cells) and $CD45RA^+$ effector memory T cells (T_{EMRA} cells), relative to those of healthy control subjects (**Fig. 1h**,**i** and **Supplementary Fig. 1d**).

Because patients present with sinopulmonary infections and had a deficiency in memory B cells and overrepresentation of transitional B cells

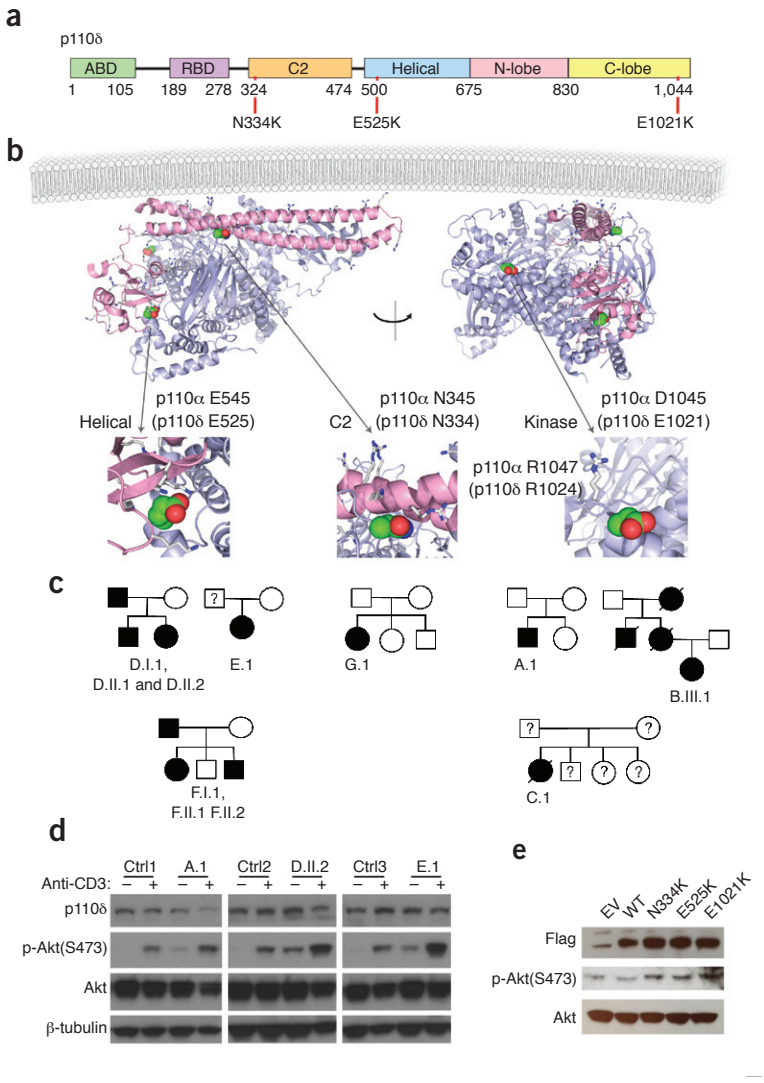

Figure 2 Heterozygosity for a gain-of-function mutation in *PIK3CD* in all affected patients results in hyperphosphorylation of Akt. (**a**) Protein domains of p110δ; red vertical lines indicate positions of substitutions. ABD, adaptor-binding domain; RDB, Ras-binding domain. (**b**) Location of substitutions (green spheres) in the structure of the H1047R mutant (blue) of human p110α (Protein Data Bank accession code, 3HHM) in complex with p85α (pink); gray sticks, positively charged amino acids along the membrane-binding face of p110; the H1047R substitution (gray sticks) is adjacent to the label 'R1047' (right). (**c**) Pedigrees of affected families: filled symbols, subjects with mutation; open symbols, unaffected subjects; ?, unscreened subjects; diagonal lines, deceased subjects. (**d**) Immunoblot analysis of p110δ, Akt phosphorylated at Ser473 (p-Akt(S473)), total Akt and β-tubulin (loading control) in serum-starved, activated T cells from three healthy control subjects (Ctrl1–Ctrl3) and patients A.1, D.II.2 and E.1, with (+) or without (–) stimulation for 10 min with anti-CD3 (quantification, **Supplementary Fig. 4a**). (**e**) Immunoblot analysis of the Flag tag, Akt phosphorylated at Ser473 and total Akt in lysates of unactivated PBMCs from healthy control subjects overexpressing empty vector (EV) or vector encoding wild-type p110δ (WT) or mutant p110δ (above lanes) at 16 h after vector transfection (quantification, **Supplementary Fig. 4f**). Data are representative four (**d**) or three (**e**) independent experiments.

(**Fig. 1d**), we further investigated those lymphocytes. We observed alterations in serum immunoglobulin concentrations in the patients, most with normal to elevated concentrations of IgM and reduced concentrations of IgA (**Supplementary Fig. 1e**). Serum concentrations of IgG were variable, but specific antibody titers were consistently low in the patients (data not shown). We observed a normal frequency of total B cells in the blood (**Supplementary Fig. 2a**) but higher expression of IgM (data not shown) and CD5 (**Supplementary Fig. 2b**), a marker whose expression is downregulated as B cells mature, on both transitional and naive B cells from patients. Consistent with the histology data (**Fig. 1c**), the contracted population of memory B cells in patients' peripheral blood had much lower frequencies of class-switched IgG^+ and IgA^+ cells (**Supplementary Fig. 2c**). *In vitro* analysis of naive B cell function revealed that they were able to undergo nearly normal proliferation in response to a variety of stimuli (**Supplementary Fig. 2d**), acquire expression of *AICDA* (which encodes the cytidine deaminase AID) (**Supplementary Fig. 2e**) and secrete IgM (**Supplementary Fig. 2f**, left). However they were impaired in secreting class-switched immunoglobulin isotypes (**Supplementary Fig. 2f**, middle and right). Memory B cells acted in a similar way, with normal secretion of IgM but impaired production of IgG and IgA (**Supplementary Fig. 2g**). Those *in vitro* findings were consistent with the *in vivo* data demonstrating diminished serum immunoglobulin and impaired humoral immune responses, which leads to susceptibility to sinopulmonary infections. Thus, this cohort of patients had combined immunodeficiency in T cells and B cells, impaired memory T cell responses with lymphoproliferation, and a striking inability to control infection with EBV and/or CMV.

Heterozygosity for gain-of-function mutations in *PIK3CD*

PIK3CD encodes the PI(3)K subunit p110δ, a protein of 1,044 amino acids with at least five domains identified by structure and function: an adaptor-binding domain, a Ras GTPase–binding domain, a PI(3)K-type C2 domain, a helical domain and a kinase domain with amino (N) and carboxyl (C) side lobes (**Fig. 2a**). Through the use of whole-exome sequencing[21] and targeted Sanger sequencing (**Supplementary Table 2**), we detected in fourteen of these patients and family members heterozygosity for one of the following three *PIK3CD* mutations, each located in a different domain (notation based on GenBank accession code NM_005026). One index patient had a C-to-A mutation at cDNA position 1002 that resulted in the amino acid substitution N334K in the C2 domain. Seven patients (three index patients plus four affected relatives, two of whom have not been fully evaluated) had a G-to-A mutation at nucleotide 1573 that resulted in an E525K substitution in the helical domain. Six patients (three index patients plus three deceased, affected relatives) had a G-to-A mutation at 3061 that resulted in an E1021K substitution in the C-lobe of the kinase domain (**Fig. 2a**,**b**). All patients with a mutation were found to have characteristics of the disease when they were evaluated. The three mutations were predicted to be damaging by functional prediction algorithms (including SIFT, PP2, LRT, MutationTaster and MutationAssessor). We suspected these were gain-of-function mutations on the basis of protein-structure analysis and comparison with homologous gain-of-function mutations in the gene encoding p110α described in human cancer cells[22] (**Supplementary Fig. 3** and **Supplementary Table 3**). Since p110δ and p110α share 72% amino acid sequence identity or similarity, as noted above, we were able to confidently map the substitutions N334K and E525K in patient p110δ to the same substitutions at the homologous residues 345 and 545, respectively, of mutant p110α already described as encoded by gain-

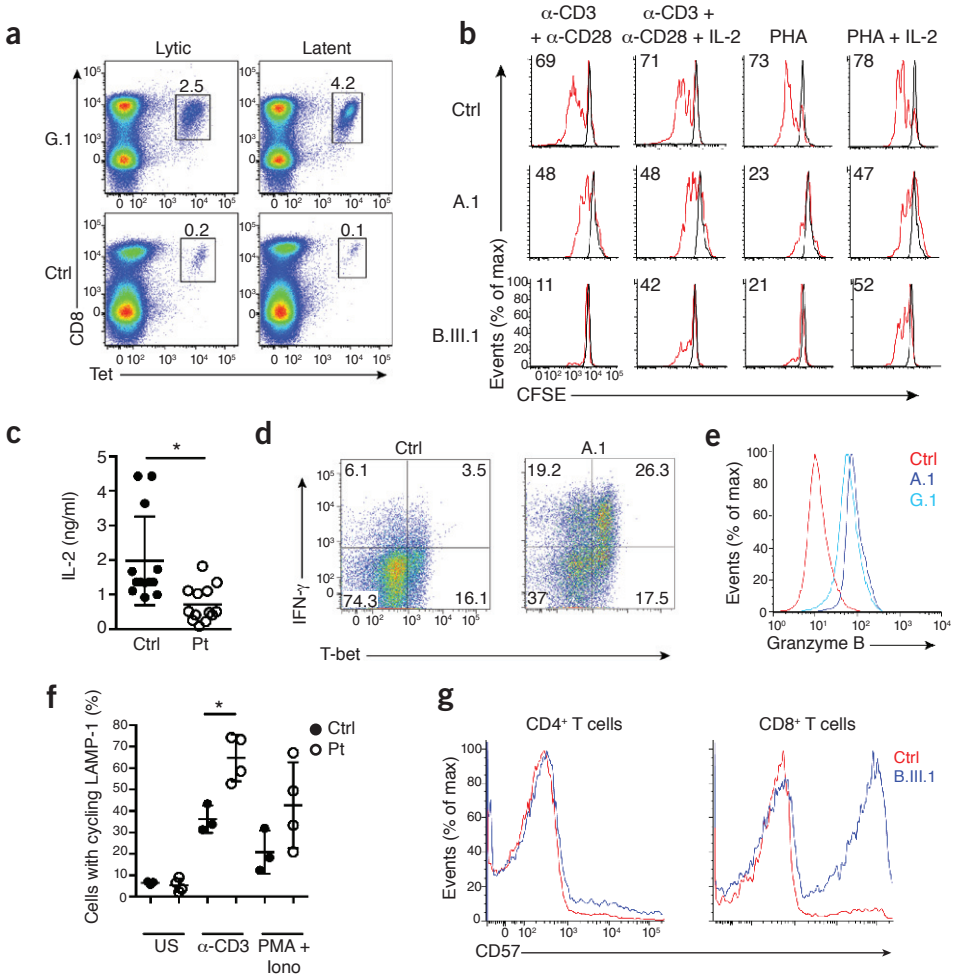

Figure 3 PBMC populations from patients include virus-specific CD8+ T cells but do not proliferate after stimulation of the TCR *in vitro* because of terminal differentiation and senescence. (**a**) Staining of EBV-specific tetramers (Tet) in PBMCs from patient G.1 and a healthy control subject for the detection of EBV lytic antigen– and EBV latent antigen–specific CD8+ T cells, assessed by flow cytometry. (**b**) Dilution of the cytosolic dye CFSE by gated CD8+ T cells among PBMCs obtained from a healthy control subject and patients A.1 and B.III.1, then stimulated for 72 h with beads coated with anti-CD3 and anti-CD28 (α-CD3 + α-CD28) alone (far left) or plus IL-2 (middle left), or with phytohemagglutinin (PHA) alone (middle right) or plus IL-2 (far right). Numbers in plots indicate percent divided cells. (**c**) Secretion of IL-2 by PBMCs activated for 48–72 h with beads coated with anti-CD3 and anti-CD28. Each symbol represents an individual healthy control subject ($n = 13$ total) or patient ($n = 13$ total); small horizontal lines indicate the mean (± s.d.). $^*P = 0.0006$ (Mann-Whitney test). (**d**) Intracellular production of interferon-γ (IFN-γ) and expression of T-bet in activated CD8+ T cells stimulated with a low dose of immobilized anti-CD3, assessed by flow cytometry (quantification, **Supplementary Fig. 5d**). (**e**) Granzyme B expression in activated CD8+ T cells from a healthy control subject and patients A.1 and G.1 (quantification, **Supplementary Fig. 5e**). (**f**) LAMP-1 cycling in CD8+ T cells left unstimulated (US) or stimulated with anti-CD3 or with the phorbol ester PMA plus ionomycin (PMA + iono), assessed by flow cytometry. Each symbol represents an individual healthy control subject ($n = 3$) or patient ($n = 4$: A.1, E.1, F.II.1 and G.1); small horizontal lines indicate the mean (± s.d.). $^*P = 0.01$ (unpaired, two-tailed *t*-test). (**g**) CD57 expression on CD4+ T cells (left) or CD8+ T cells (right) from a healthy control subject and patient B.III.1 (quantification, **Supplementary Fig. 5h**). Data are representative of four independent experiments (**a**,**c**), six independent experiments with a total of eight patients (**b**), two independent experiments (**d**–**f**) or three independent experiments with four different patients (**g**).

of-function mutations in cancer[22–25]. The substitution E1021K (in the kinase domain) has been reported before in a boy with primary B cell immunodeficiency[26]. Glu1021 of p110δ corresponds to Asp1045 of p110α, which is two residues upstream of a known gain-of-function substitution (H1047R in p110α; **Fig. 2b**) that reportedly increases the interaction of p110α with the cell membrane and thereby increases its activity by enhancing accessibility of the binding site to PtdIns(4,5)P_2 (ref. 23). The substitution of glutamic acid with lysine at residue 1021 of p110δ (E1021K) resulted in a change in the logarithmic acid dissociation constant (pK_a) of +6.28, similar to the change in pK_a that results from the histidine-to-arginine substitution at residue 1047 of p110α (H1047R; +6.48); this indicates the same increased propensity for interaction with the negatively charged phospholipid head groups of the inner leaflet of the plasma membrane. Moreover, two additional reports have demonstrated that the H1047R substitution of p110α mimics binding to Ras-GTP to augment the catalytic activity of PI(3)K[25] and affects the conformation of the activation loop to promote kinase activity[22], which suggests that the E1021K substitution of p110δ in our patients may have multiple gain-of-function effects.

We confirmed that only two of the seven families had a *de novo* mutation in the index patient, and another three had confirmed affected members in multiple generations (**Fig. 2c**). For the remaining two families, specimens from one or both parents were not accessible. The appearance of *PIK3CD* mutations in three different sites among seven unrelated families from different ethnic and racial backgrounds (**Supplementary Table 1**) eliminated the possibility of a founder effect, while the presence of the same mutation in multiple families suggested the occurrence of mutational 'hot spots', as seen before in genetic diseases of the immune system[27,28].

Next we sought to evaluate expression of p110δ and test the hypothesis that PI(3)K was hyperactive in our patients. We examined abundance of p110δ protein and phosphorylation of Akt at Ser473 in T cell blasts and peripheral blood mononuclear cells (PBMCs) from patients (**Fig. 2d** and **Supplementary Fig. 4a–c**). Expression of the each of the three mutant p110δ proteins was normal; however, phosphorylation of Akt was higher than that in cells from healthy control subjects, before and after stimulation with antibody to CD3 (anti-CD3) (**Supplementary Fig. 4a**,**c**). We also found that phosphorylation of Akt at Thr308 was higher in T cell blasts from patients than in those from healthy control subjects (**Supplementary Fig. 4d**,**e**). Moreover, the abundance of Foxo1, a substrate of Akt that is degraded when phosphorylated, was lower in T cell blasts from patients than in those from healthy control subjects, as assessed by immunoblot analysis (data not shown). To confirm that substitutions in p110δ were responsible for the hyperactivation of Akt, we overexpressed N334K, E525K or

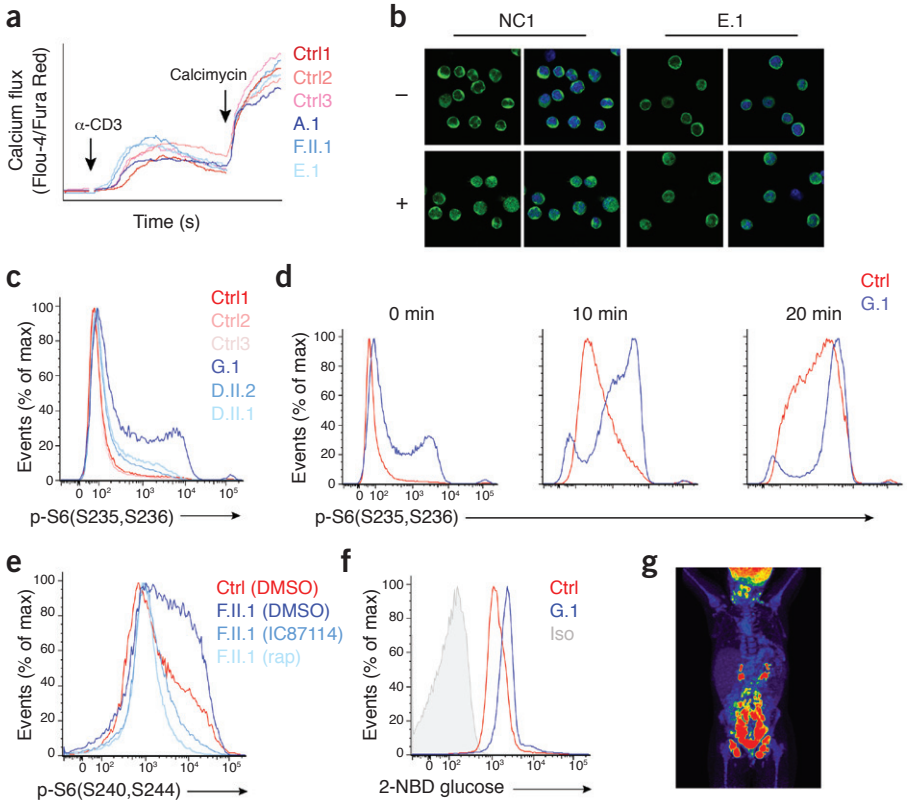

Figure 4 T cells from patients exhibit normal TCR signaling responses but elevated mTOR activity and glucose uptake *in vitro*. (**a**) Calcium flux induced by stimulation (downward arrows) with anti-CD3 and the calcium ionophore calcimycin (positive control) in T cell blasts from healthy control subjects (Ctrl1–Ctrl3) and patients (A.1, E.1 and F.II.1), measured as the ratio of the fluorescent Ca^{2+} indicators Fluo-4 and Fura Red. (**b**) Confocal microscopy of the translocation of p65 (green; left of each pair) into the nucleus (stained blue with the DNA-intercalating dye DAPI; merged in right of each pair) in serum-starved T cell blasts left unstimulated (–) or stimulated via the TCR (+). (**c**,**d**) Phosphorylation of S6 at Ser235 and Ser236 (p-S6(S235,S236)) in unstimulated T cell blasts (fixed in complete medium) from healthy control subjects (Ctrl1–Ctrl3) and patients (G.1, D.II.1 and D.II.2) (**c**) or in cells from a healthy control subject and patient G.1 at baseline (0 min) and 10 min or 20 min after stimulation with anti-CD3 plus protein A (**d**), analyzed by flow cytometry (quantification (for **c**), **Supplementary Fig. 8a**). (**e**) Phosphorylation of S6 at residues Ser240 and Ser244 (p-S6(S240,S244)) in unstimulated T cell blasts obtained from a healthy control subject and patient F.II.1 and treated for 20 min with dimethyl sulfoxide (DMSO), 10 μM IC87114 (p110δ inhibitor) or 50 nM rapamycin (rap; mTOR inhibitor). (**f**) Glucose uptake in glucose-starved T cell blasts from a healthy control subject and patient G.1, measured by flow cytometry analysis of the fluorescent deoxyglucose analog 2-NBDG (quantification, **Supplementary Fig. 8c**). Iso, isotype-matched control antibody. (**g**) Positron-emission tomography scanning of patient G.1 after administration of the glucose analog ^{18}F-fludeoxyglucose, showing glucose uptake. Data are representative of two independent experiments with five different healthy control subjects and five different patients (**a**), one experiment with three healthy control subjects and three patients (**b**), three independent experiments (**c**,**e**), two independent experiments (**d**), five independent experiments (**f**) or three independent experiments with one patient in each (**g**).

E1021K mutant p110δ in PBMCs from healthy control subjects and found that the mutant p110δ proteins induced hyperphosphorylation of Akt (**Fig. 2e** and **Supplementary Fig. 4f**). We also confirmed that result by overexpression of mutant p110δ in the H9 human T cell line (**Supplementary Fig. 4g**). Moreover, we found that mutant p110δ was able to interact with the p85α subunit as well as wild-type p110δ did, as assessed by overexpression and coimmunoprecipitation (**Supplementary Fig. 4h**). Thus, each subject in our patient cohort was heterozygous for an inherited or *de novo* gain-of-function mutation in the gene encoding p110δ that led to expression of a hyperactive kinase that augmented the phosphorylation of Akt.

Expanded senescent CD8$^+$ effector T cell populations

We next assessed the frequency of EBV-specific CD8$^+$ T cells by staining PBMCs *ex vivo* with HLA tetramers loaded with lytic or latent EBV peptide antigens. Despite their uncontrolled infection with EBV, these patients generated normal to high frequencies of EBV-specific CD8$^+$ T cells (**Fig. 3a** and **Supplementary Fig. 5a**). Tetramer-positive CD8$^+$ T cells had an effector memory phenotype (CCR7$^-$CD45RA$^-$) and were more activated, as shown by upregulation of expression of the costimulatory molecule CD38, than were cells from healthy control subjects (**Supplementary Fig. 5b**,**c**). These data suggested that the *PIK3CD* mutations were unlikely to result in global impairment of the *in vivo* recognition of antigen by T cells.

Phenotypically, CD8$^+$ T cells from patients appeared to be predominantly negative for expression of the chemokine receptor CCR7 (**Fig. 1h** and **Supplementary Fig. 1d**), which suggested a terminally differentiated state. Correspondingly, *in vitro* activation of unsorted PBMCs with various stimuli revealed a reduced proliferative capacity and diminished secretion of interleukin 2 (IL-2) relative to those of cells from healthy controls, but activation of isolated naive CD4$^+$ T cells did not (**Fig. 3b**,**c** and data not shown); however, the proliferation defect was 'rescued' by stimulation with beads coated with anti-CD2, anti-CD3 and anti-CD28 or with allogeneic PBMCs plus phytohemagglutinin (data not shown). As the composition of cells in the peripheral blood of patients was biased toward effector T cells, the defective proliferation was consistent with the well-described ability of naive T cells to proliferate better than differentiated effector cells. Also consistent with a T_{EM} cell and/or T_{EMRA} cell phenotype, activated patient CD8$^+$ T cells exhibited characteristics of enhanced effector function. We found that expression of interferon-γ, the transcription factor T-bet and granzyme B, as well as degranulation (as reflected by cycling of LAMP-1 (CD107a) after stimulation), were higher in cytotoxic T lymphocytes cultured from patients than in those from healthy control subjects (**Fig. 3d–f** and **Supplementary Fig. 5d–f**). We also assessed granzyme B expression after activation of purified naive CD8$^+$ T cells and again observed higher expression in cells from patients than in those from healthy control subjects (data not shown). When we assessed the cytotoxic function of cytotoxic T lymphocytes from patients by anti-CD3-mediated redirected lysis of target cells (of the P815 mouse lymphoblast-like mastocytoma cell line), cells from patients exhibited a normal capacity to kill

(**Supplementary Fig. 5g**). Notably, we found that expression of the senescence-associated marker CD57 was significantly higher on $CD8^+$ T cells, but not on $CD4^+$ T cells, from patients than on their counterparts from healthy control subjects[29] (**Fig. 3g**, **Table 1** and **Supplementary Fig. 5h**). Of note, we observed normal to high expression of the cytotoxic lymphocyte–activating receptor NKG2D (data not shown) and variable expression of the T cell inhibitory receptor PD-1 on $CD8^+$ T cells from patients (**Supplementary Fig. 6**). Hence, phenotypically and functionally, patient $CD8^+$ T cells were mostly T_{EM} cells and/or T_{EMRA} cells with a low proliferative capacity but with certain aspects of high effector function characteristic of senescent effector cells.

Augmented mTOR signaling and glycolysis

To gain insight into how the p110δ gain-of-function substitutions caused terminal differentiation and senescence, we examined signaling pathways downstream of PI(3)K. T cell antigen receptor (TCR)-induced calcium flux and translocation of the transcription factor NF-κB subunit p65 to the nucleus were normal in T cell blasts from patients (**Fig. 4a**,**b**), which demonstrated that multiple aspects of TCR signaling were intact. Moreover, the expression of PTEN, the cell-cycle inhibitor $p27^{Kip1}$ and other signaling molecules was normal in T cells from patients (**Supplementary Fig. 7**). An important molecule activated downstream of PI(3)K and Akt in many cell types is mTOR, a serine-threonine kinase that modulates T cell metabolism and the effector differentiation of $CD8^+$ T cells through the induction of glycolysis. We therefore hypothesized that hyperactive PI(3)K-Akt signaling was affecting T cell metabolism by stimulating the mTOR pathway. Consistent with our hypothesis, we observed more phosphorylation of the ribosomal protein S6 at Ser235 and Ser236 downstream of mTOR in activated cells from patients than in those from healthy control subjects (**Fig. 4c**,**d** and **Supplementary Fig. 8a**), and that was true even in purified and activated naive $CD8^+$ T cells (data not shown). To confirm that the increased phosphorylation of S6 in cells from patients was achieved via mTORC1, we also examined the extent of phosphorylation at the mTORC1-specific[30] sites Ser240 and Ser244 of S6. Similar to the sites Ser235 and Ser236, the sites Ser240 and Ser244 on S6 were hyperphosphorylated in cultured T cell blasts from patients (**Fig. 4e**). Moreover, that phosphorylation was greatly diminished by inhibition of either p110δ or mTORC1 through the use of IC87114 or rapamycin, respectively (**Fig. 4e**), which supported the conclusion that hyperactive PI(3)K drove the hyperactivation of mTOR in cells from patients. As further support of that conclusion, we measured the phosphorylation of S6 at Ser235 and Ser236 in cells preincubated in phosphate-buffered saline (PBS) for removal of the glucose and amino acids needed to maintain mTOR activity. Indeed, we found that the observed hyperphosphorylation of S6 was lost under those conditions (**Supplementary Fig. 8b**), consistent with a requisite role for mTOR in the hyperphosphorylation of S6. As hypothesized from the hyperactivation of mTORC1, glucose uptake was augmented in T cell blasts from patients with mutant p110δ relative to that in cells from healthy control subjects (**Fig. 4f** and **Supplementary Fig. 8c**). Increased glucose uptake was also evident in the lymph nodes (most pronounced in the iliac chains and inguinal regions bilaterally) of patient G.1, as evaluated by positron-emission tomography scanning (**Fig. 4g**), which suggested that mutant p110δ drove the T cells into glycolytic metabolism. Notably, the patients with the most hyperphosphorylation of S6 and greatest glucose uptake (A.1 and G.1) were also the most severely affected clinically. Thus, activating p110δ substitutions were associated with hyperactivity of the PI(3)K-Akt-mTOR signaling pathway in T cells, which led to enhanced glycolysis; this provided a mechanism for the predisposition to senescence.

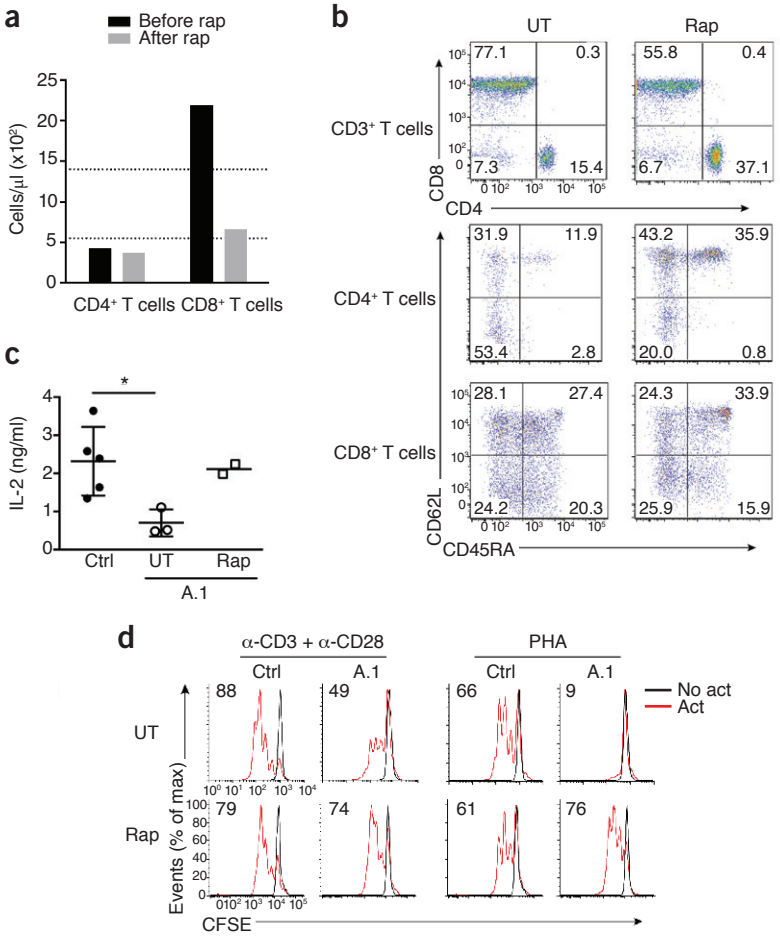

Figure 5 *In vivo* treatment with rapamycin improves disease phenotypes *in vitro* and *in vivo*. (**a**) Quantification of $CD4^+$ or $CD8^+$ T cells from patient A.1 before and after treatment with rapamycin; dotted lines indicate the range of T cell counts for healthy control subjects. (**b**) Flow cytometry of PBMCs from patient A.1, left untreated (UT) or treated *in vivo* with rapamycin (Rap), and stained for CD8 versus CD4 ($CD3^+$ gate (top)) or for CD62L versus CD45RA ($CD4^+$ gate (middle) or $CD8^+$ gate (bottom)). (**c**) *In vitro* production of IL-2 by PMBCs obtained from an untreated healthy control subject ($n = 5$ independent measurements) or patient A.1 before (UT; $n = 3$ independent measurements) and after (Rap; $n = 2$ independent measurements) treatment with rapamycin, then activated for 24 h with beads coated with anti-CD3 and anti-CD28. Each symbol represents an independent measurement; small horizontal lines indicate the mean (± s.d.). $^*P = 0.04$ (Mann-Whitney test). (**d**) Proliferation of PBMCs obtained from a healthy control subject or patient A.1 before (top) or after (bottom) *in vivo* treatment with rapamycin, then left unactivated (No act) or activated (Act) for 72 h with beads coated with anti-CD3 and anti-CD28 or with phytohemagglutinin (presented as in **Fig. 3b**). Data are representative of three experiments (**a**,**b**,**d**) or three (UT) or two (Rap) independent experiments (**c**).

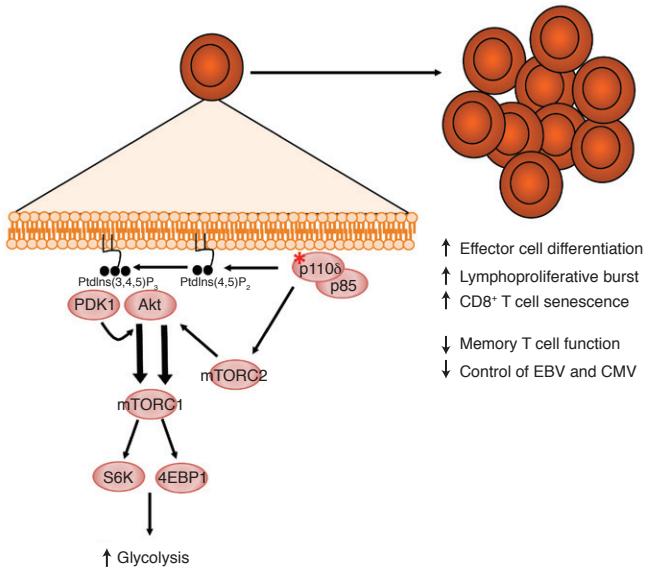

Figure 6 Proposed model for the effects of activating substitutions (red asterisk) in p110δ. Augmented PI(3)K signaling results in increased glycolysis, which causes $CD8^+$ T cells to differentiate into effector cells that proliferate vigorously and then senesce. This results in the impaired generation of functional, long-lived memory $CD8^+$ T cells and, consequently, poor control of infection with EBV and/or CMV.

Treatment of disease with rapamycin

As aerobic glycolysis is induced after T cell activation[6] and is incompatible with the maintenance of resting naive T cells[12], we hypothesized that *in vivo* treatment of patients who express mutant p110δ with rapamycin to inhibit mTOR (and therefore glycolysis) would enable the persistence of naive T cells. After treating patient A.1 (the most severely affected patient with extreme lymphoproliferation) with rapamycin (maintaining trough drug concentrations of 15 ng/ml), we observed a reduction in $CD8^+$ T cell counts to normal numbers within approximately 4 months and noted an increase in the frequency of naive T cells among PBMCs (**Fig. 5a**,**b**). That effect was specific, as $CD4^+$ T cells, which did not expand their populations in the patients, showed no decrease in number after rapamycin therapy (**Fig. 5a**). Consistent with the 'rescue' of naive T cells in the peripheral blood, we found nearly complete restoration of IL-2 secretion and proliferative responses after *in vitro* TCR ligation (**Fig. 5c**,**d**). Clinically, we observed a reduction in hepatosplenomegaly and lymphadenopathy (**Supplementary Fig. 9**). Thus, *in vivo* administration of an mTOR inhibitor improved the derangements of the immune system induced by gain-of-function mutation of the gene encoding p110δ by modulating the cell populations in patient blood to restore a more normal balance of naive, effector and memory $CD8^+$ T cell populations. Together these data support the hypothesis that enhanced activity of p110δ due to a genetic alteration elicits a lymphoproliferative immunodeficiency caused by mTOR-dependent skewing of T cells to a senescent effector phenotype (**Fig. 6**), which can be reversed pharmacologically by rapamycin.

DISCUSSION

Studies of animal models have suggested that impaired PI(3)K signaling leads to immunodeficiency and inflammation, whereas unrestrained PI(3)K signaling contributes to autoimmunity and hematological malignancy[1]. However, that simplistic dichotomy does not fully explain the effects of PI(3)K. Mice that express a catalytically inactive form of p110δ exhibit impaired antigen receptor signaling in B cells and T cells and attenuated immune responses but also develop inflammatory bowel disease[31]. Moreover, mice that lack p85α show impaired development and activation of B cells but normal activation of T cells under the conditions tested[32,33]. Similarly, patients deficient in the p85α subunit of PI(3)K also lack B cells and serum immunoglobulins[34]. T cell–specific deletion of PTEN in mice results in hyperactivation of the PI(3)K pathway and causes a lethal lymphoproliferative disease[35]. In human cancers, activating mutations in genes encoding PI(3)K proteins (most frequently p110α) are common, consistent with the role of these proteins in proliferation and survival[36,37]. Enhanced PI(3)K activity has also been observed in hematopoietic cancers due to oncogenic activation of upstream regulators[38], which has prompted investigation of p110δ-specific inhibitors for therapeutic use[39]. However, the full phenotypic effect of inherited lesions in *PIK3CD* in humans has not been described. We have now reported the identification of patients heterozygous for one of three different germline mutations in *PIK3CD* in a cohort of fourteen patients from seven families with an unusual combination of lymphoproliferation and immunodeficiency.

Our patients generally presented in childhood with combined immunodeficiency in T cells and B cells and peripheral expansion of lymphocyte populations. A major hallmark of this disease is the appearance of T cell– and B cell–positive lymphoid nodules on respiratory and gastrointestinal mucosal surfaces, a phenotype that is notable given data linking PI(3)K and Akt to the regulation of T cell trafficking[40]. We noted generally low $CD4^+$ T cell counts, and we observed profound defects in mitogen and antigen recall responses. Common to all patients were viremia due to EBV and/or CMV (consistent with T cell defects) and recurrent sinopulmonary infections (consistent with humoral defects). The B cell abnormalities included the accumulation of transitional B cells, a paucity of memory B cells and defects in the secretion of class-switched immunoglobulins, consistent with a role for PI(3)K in the development and maturation of B cells[41,42]. EBV^+ lymphoma was diagnosed in two patients, and an additional two patients in these families died from lymphoma before our discovery of this genetic lesion. Investigation of patients who share this phenotype revealed three different gain-of-function mutations in *PIK3CD*. By structural comparison to the p110α mutants encoded by gain-of-function mutations, we surmised that the substitutions E525K (in the helical domain) and N334K (in the C2 domain) in p110δ of our patients probably disrupt specific inhibitory contacts between p110δ and the inter-SH2 and N-terminal SH2 domains of p85α, respectively[5,23,24,43]. In contrast, the E1021K substitution of p110δ in our patients probably enhances the recruitment of p110δ to the plasma membrane and increases its catalytic activity[22,23,25].

Because our patients are unable to control infection with EBV and/or CMV , we focused our studies on $CD8^+$ T cells and unexpectedly found that total and virus-specific $CD8^+$ T cell populations were expanded, with enrichment for phenotypically antigen-experienced $CD8^+$ T cells. However, we observed that patient $CD8^+$ T cells were severely impaired in *in vitro* proliferation and IL-2 secretion despite hyperphosphorylation of Akt. Akt activity is widely known to promote cell growth, proliferation and metabolism, hence its major role in tumorigenesis[36]. Thus, we were initially surprised that hyperactivation of this pathway resulted in an immunodeficiency with profound defects in *in vitro* T cell proliferation and IL-2 production. On closer examination, we found that many aspects of TCR signaling were intact but that T cells from patient blood were skewed toward senescent ($CD57^+$) and terminally differentiated T_{EMRA} or T_{EM} cells. Thus, we hypothesized that the hyperactive p110δ-Akt-mTOR pathway was promoting aerobic glycolysis

(the Warburg effect[7,8]), limiting the function and survival of memory T cells[6,7,12,17] and driving the senescence of CD8$^+$ T cells[15,44]. Indeed, our patients exhibited p110δ- and mTOR-dependent hyperphosphorylation of S6 and increased glucose uptake by cultured T cell blasts, which confirmed that cell-intrinsic mTOR signaling was enhanced by the gain-of-function mutations in these patients. Thus, over time, patients respond ineffectively to infections by inducing the terminal differentiation of CD8$^+$ T cells into senescent effector cells without supporting the development of functional long-lived memory cells. As it is widely accepted that memory T cells are critical for control of chronic infections, the poor anti-EBV and anti-CMV immunity of our patients is probably at least partially due to a diminished pool of functional long-lived memory CD8$^+$ T cells[45]. Additionally, the mTOR-driven differentiation into effector cells could explain the lymphadenopathy, as skewing toward effector-type cells may result in an enhanced proliferative burst upon encounter with antigen.

The data reported above provided a rationale for the use of rapamycin therapy to inhibit mTOR, similar to interventions in specific cancers[46]. Although our experience with this intervention is limited at present, in patient A.1, rapamycin produced notable clinical improvement in lymphoproliferation and was associated with nearly normalization of peripheral T cell populations as well as better proliferation and IL-2 secretion by CD8$^+$ T cells *in vitro*. The restoration of naive T cell and T_{CM} cell populations supports our hypothesis that metabolic effects of mTOR have a central role in causing immunodeficiency. These findings raise the possibility that p110δ-specific inhibitors that have described[47] would also be effective in treating this disease clinically and may in fact have better efficacy than rapamycin, as other, mTOR-independent pathways downstream of PI(3)K would also be targeted.

Although the possibility exists that chronic infection with EBV and/or CMV contributed to the appearance of CD57$^+$ CD8$^+$ T cells, we were unable to find a correlation between viral load and skewing of CD8$^+$ T cells. Our studies of another immunodeficiency associated with EBV, XMEN disease, have revealed normal CD57 expression on CD8$^+$ T cells despite viral loads higher than those noted in the disease described here (data not shown). We also noted that the patients most affected clinically (A.1 and G.1) also had signs of the greatest mTOR activity (i.e., phosphorylation of S6 and glucose uptake). Moreover, treatment with rapamycin partially normalized T cell populations, which again supported the proposal of a cell-intrinsic, mTOR-driven mechanism of effector differentiation and senescence rather than effects of chronic viremia.

In conclusion, we have identified a previously unknown human immunodeficiency we have called 'PASLI disease' ('p110δ-activating mutation causing senescent T cells, lymphadenopathy and immunodeficiency'). This disease is caused by dominant, gain-of-function mutations in *PIK3CD* that promote mTOR-mediated intrinsic CD8$^+$ T cell defects that explain, at least partially, the immunological phenotypes of such patients. Our findings position p110δ as a critical participant in the regulation of immunity in humans.

Note added in proof: Another study has now independently described a cohort of patients with the E1021K substitution of p110δ[48].

METHODS

Methods and any associated references are available in the online version of the paper.

Accession codes. Online Mendelian Inheritance in Man: p110δ, 602839.

Note: Any Supplementary Information and Source Data files are available in the online version of the paper.

ACKNOWLEDGMENTS

We thank the referring physicians, as well as the patients and families. Supported by the Division of Intramural Research, National Institute of Allergy and Infectious Diseases, Clinical Center of the US National Institutes of Health (C.L.L., H.S.K., J.E.N., M.B., J.S., W.O., V.K.R., A.A., A.A.H., K.N.O., T.A.F., S.P., S.M.H., J.I.C., M.J.L., G.U.), the National Human Genome Research Institute of the US National Institutes of Health (F.Z., J.L.C., P.L.S.), the Frederick National Laboratory for Cancer Research of the US National Institutes of Health (HHSN261200800001E), the National Health and Medical Research Council of Australia (E.K.D., U.P., S.G.T.), Cancer Council NSW (S.G.T.), the Cancer Institute NSW (U.P.), the Research Foundation-Flanders, Belgium (L.M.) and the National Institute of General Medical Sciences (C.L.L. and R.Z.). The content of this publication does not necessarily reflect the views or policies of the US Department of Health and Human Services, nor does mention of trade names, commercial products or organizations imply endorsement by the US Government.

AUTHOR CONTRIBUTIONS

C.L.L did experiments, analyzed data and developed and wrote the manuscript; H.S.K., F.Z., E.K.D., U.P., D.T.A., L.M. and J.L.C. did experiments and analyzed data; J.E.N. analyzed genomic DNA sequencing and bioinformatics, discovered candidate genes and analyzed protein structure; M.B. analyzed p110 structure; J.S. did experiments and analyzed genomic DNA sequencing and data; W.O. did experiments; D.M.F. supervised research and data analysis; V.K.R. evaluated patients and collected data; T.P.A. and J.I.C. provided patient access, clinical data, samples and advice; A.A. evaluated patients and collected and analyzed data; A.A.H. coordinated patient access, data collection and analysis; L.R.F. evaluated and prepared data from clinical imaging studies; K.N.O. evaluated patients and collected and analyzed data; T.A.F. supervised research and data analysis and provided advice; S.P. did histological and immunohistochemical analyses of patient samples; S.M.H. supervised research and data analysis and provided advice; J.B.O planned and supervised whole-exome sequencing experiments; S.G.T. planned and supervised experiments, analyzed data, provided advice and prepared the manuscript; P.L.S. planned and supervised experiments, analyzed data and provided advice; M.J.L. supervised research and data analysis, provided advice and prepared the manuscript; G.U. coordinated research efforts, supervised research work and data analysis, and prepared the manuscript; and all authors discussed and revised the manuscript.

COMPETING FINANCIAL INTERESTS

The authors declare no competing financial interests.

1. Okkenhaug, K. & Vanhaesebroeck, B. PI3K in lymphocyte development, differentiation and activation. *Nat. Rev. Immunol.* **3**, 317–330 (2003).
2. Hemmings, B.A. & Restuccia, D.F. PI3K-PKB/Akt pathway. *Cold Spring Harb. Perspect. Biol.* **4**, a011189 (2012).
3. Chantry, D. *et al.* p110δ, a novel phosphatidylinositol 3-kinase catalytic subunit that associates with p85 and is expressed predominantly in leukocytes. *J. Biol. Chem.* **272**, 19236–19241 (1997).
4. Vanhaesebroeck, B. *et al.* P110δ, a novel phosphoinositide 3-kinase in leukocytes. *Proc. Natl. Acad. Sci. USA* **94**, 4330–4335 (1997).
5. Huang, C.H. *et al.* The structure of a human p110α/p85α complex elucidates the effects of oncogenic PI3Kα mutations. *Science* **318**, 1744–1748 (2007).
6. Gubser, P.M. *et al.* Rapid effector function of memory CD8 T cells requires an immediate-early glycolytic switch. *Nat. Immunol.* **14**, 1064–1072 (2013).
7. Xu, X., Ye, L., Araki, K. & Ahmed, R. mTOR, linking metabolism and immunity. *Semin. Immunol.* **24**, 429–435 (2012).
8. Yang, K. & Chi, H. mTOR and metabolic pathways in T cell quiescence and functional activation. *Semin. Immunol.* **24**, 421–428 (2012).
9. Zinzalla, V., Stracka, D., Oppliger, W. & Hall, M.N. Activation of mTORC2 by association with the ribosome. *Cell* **144**, 757–768 (2011).
10. Alessi, D.R. *et al.* Characterization of a 3-phosphoinositide-dependent protein kinase which phosphorylates and activates protein kinase Bα. *Curr. Biol.* **7**, 261–269 (1997).
11. Sarbassov, D.D., Guertin, D.A., Ali, S.M. & Sabatini, D.M. Phosphorylation and regulation of Akt/PKB by the rictor-mTOR complex. *Science* **307**, 1098–1101 (2005).
12. Kaech, S.M. & Cui, W. Transcriptional control of effector and memory CD8$^+$ T cell differentiation. *Nat. Rev. Immunol.* **12**, 749–761 (2012).
13. Finlay, D.K. *et al.* PDK1 regulation of mTOR and hypoxia-inducible factor 1 integrate metabolism and migration of CD8$^+$ T cells. *J. Exp. Med.* **209**, 2441–2453 (2012).
14. Fox, C.J., Hammerman, P.S. & Thompson, C.B. Fuel feeds function: energy metabolism and the T-cell response. *Nat. Rev. Immunol.* **5**, 844–852 (2005).
15. Astle, M.V. *et al.* AKT induces senescence in human cells via mTORC1 and p53 in the absence of DNA damage: implications for targeting mTOR during malignancy. *Oncogene* **31**, 1949–1962 (2012).

16. Kim, E.H. & Suresh, M. Role of PI3K/Akt signaling in memory CD8 T cell differentiation. *Front. Immunol.* **4**, 20 (2013).
17. Araki, K. *et al.* mTOR regulates memory CD8 T-cell differentiation. *Nature* **460**, 108–112 (2009).
18. Kim, E.H. *et al.* Signal integration by Akt regulates CD8 T cell effector and memory differentiation. *J. Immunol.* **188**, 4305–4314 (2012).
19. Sukumar, M. *et al.* Inhibiting glycolytic metabolism enhances CD8$^+$ T cell memory and antitumor function. *J. Clin. Invest.* **123**, 4479–4488 (2013).
20. Jarrett, A.F., Armstrong, A.A. & Alexander, E. Epidemiology of EBV and Hodgkin's lymphoma. *Ann. Oncol.* **7** (suppl. 4), 5–10 (1996).
21. Berndt, A. *et al.* The p110 δ structure: mechanisms for selectivity and potency of new PI(3)K inhibitors. *Nat. Chem. Biol.* **6**, 117–124 (2010).
22. Bader, A.G., Kang, S., Zhao, L. & Vogt, P.K. Oncogenic PI3K deregulates transcription and translation. *Nat. Rev. Cancer* **5**, 921–929 (2005).
23. Mandelker, D. *et al.* A frequent kinase domain mutation that changes the interaction between PI3Kα and the membrane. *Proc. Natl. Acad. Sci. USA* **106**, 16996–17001 (2009).
24. Wu, H. *et al.* Regulation of Class IA PI 3-kinases: C2 domain-iSH2 domain contacts inhibit p85/p110α and are disrupted in oncogenic p85 mutants. *Proc. Natl. Acad. Sci. USA* **106**, 20258–20263 (2009).
25. Zhao, L. & Vogt, P.K. Helical domain and kinase domain mutations in p110α of phosphatidylinositol 3-kinase induce gain of function by different mechanisms. *Proc. Natl. Acad. Sci. USA* **105**, 2652–2657 (2008).
26. Jou, S.T. *et al.* Identification of variations in the human phosphoinositide 3-kinase p110δ gene in children with primary B-cell immunodeficiency of unknown aetiology. *Int. J. Immunogenet.* **33**, 361–369 (2006).
27. Damgaard, R.B. *et al.* Disease-causing mutations in the XIAP BIR2 domain impair NOD2-dependent immune signalling. *EMBO Mol. Med.* **5**, 1278–1295 (2013).
28. Li, F.Y. *et al.* Second messenger role for Mg^{2+} revealed by human T-cell immunodeficiency. *Nature* **475**, 471–476 (2011).
29. Brenchley, J.M. *et al.* Expression of CD57 defines replicative senescence and antigen-induced apoptotic death of CD8$^+$ T cells. *Blood* **101**, 2711–2720 (2003).
30. Roux, P.P. *et al.* RAS/ERK signaling promotes site-specific ribosomal protein S6 phosphorylation via RSK and stimulates cap-dependent translation. *J. Biol. Chem.* **282**, 14056–14064 (2007).
31. Okkenhaug, K. *et al.* Impaired B and T cell antigen receptor signaling in p110δ PI 3-kinase mutant mice. *Science* **297**, 1031–1034 (2002).
32. Fruman, D.A. *et al.* Impaired B cell development and proliferation in absence of phosphoinositide 3-kinase p85α. *Science* **283**, 393–397 (1999).
33. Suzuki, H. *et al.* Xid-like immunodeficiency in mice with disruption of the p85alpha subunit of phosphoinositide 3-kinase. *Science* **283**, 390–392 (1999).
34. Conley, M.E. *et al.* Agammaglobulinemia and absent B lineage cells in a patient lacking the p85alpha subunit of PI3K. *J. Exp. Med.* **209**, 463–470 (2012).
35. Suzuki, A. *et al.* T cell-specific loss of Pten leads to defects in central and peripheral tolerance. *Immunity* **14**, 523–534 (2001).
36. Denley, A., Kang, S., Karst, U. & Vogt, P.K. Oncogenic signaling of class I PI3K isoforms. *Oncogene* **27**, 2561–2574 (2008).
37. Zhao, L. & Vogt, P.K. Class I PI3K in oncogenic cellular transformation. *Oncogene* **27**, 5486–5496 (2008).
38. Vivanco, I. & Sawyers, C.L. The phosphatidylinositol 3-kinase AKT pathway in human cancer. *Nat. Rev. Cancer* **2**, 489–501 (2002).
39. Billottet, C. *et al.* A selective inhibitor of the p110 δ isoform of PI 3-kinase inhibits AML cell proliferation and survival and increases the cytotoxic effects of VP16. *Oncogene* **25**, 6648–6659 (2006).
40. Sinclair, L.V. *et al.* Phosphatidylinositol-3-OH kinase and nutrient-sensing mTOR pathways control T lymphocyte trafficking. *Nat. Immunol.* **9**, 513–521 (2008).
41. Omori, S.A. *et al.* Regulation of class-switch recombination and plasma cell differentiation by phosphatidylinositol 3-kinase signaling. *Immunity* **25**, 545–557 (2006).
42. Srinivasan, L. *et al.* PI3 kinase signals BCR-dependent mature B cell survival. *Cell* **139**, 573–586 (2009).
43. Amzel, L.M. *et al.* Structural comparisons of class I phosphoinositide 3-kinases. *Nat. Rev. Cancer* **8**, 665–669 (2008).
44. Yentrapalli, R. *et al.* The PI3K/Akt/mTOR pathway is implicated in the premature senescence of primary human endothelial cells exposed to chronic radiation. *PLoS ONE* **8**, e70024 (2013)
45. Gourley, T.S., Wherry, E.J., Masopust, D. & Ahmed, R. Generation and maintenance of immunological memory. *Semin. Immunol.* **16**, 323–333 (2004).
46. Faivre, S., Kroemer, G. & Raymond, E. Current development of mTOR inhibitors as anticancer agents. *Nat. Rev. Drug Discov.* **5**, 671–688 (2006).
47. Lannutti, B.J. *et al.* CAL-101, a p110δ selective phosphatidylinositol-3-kinase inhibitor for the treatment of B-cell malignancies, inhibits PI3K signaling and cellular viability. *Blood* **117**, 591–594 (2011).
48. Angulo, I. *et al.* Phosphoinositide 3-kinase δ gene mutation predisposes to respiratory infection and airway damage. *Science* doi:10.1126/science.1243292 (17 October 2013).

ONLINE METHODS

Human subjects and rapamycin therapy. All human subjects (or their guardians) in this study provided written informed consent in accordance with Helsinki principles for enrollment in research protocols (clinical trials registration number NCT00001355) that were approved by the Institutional Review Board of the National Institute of Allergy and Infectious Diseases (US National Institutes of Health). Blood from healthy donors was obtained at the NIH Clinical Center under approved protocols. Mutations will be automatically archived by Online Mendelian inheritance in Man (accession code, 602839). We will also create a web page through the National Center for Biotechnology Information (NCBI) to accumulate patient mutation data in the format of the Leiden Online Variant Database as patients are identified. Patient A.1 was treated with once daily oral rapamycin at a dose of 1 mg, with the initial calculation based on 1 mg per m^2 surface area and subsequently adjusted to maintain a serum trough concentration of 12–15 ng/ml. All procedures were based on standard of care, and established clinical guidelines were followed.

Histology. Tissue biopsies were fixed with formalin and embedded in paraffin, followed by immunohistochemical staining with antibody to EBV LMP1 (CS 1-4; Dako), IgG (A0423; Dako) and IgM (A0425; Dako). Samples were stained on an automated system (BenchMark, XT) according to the manufacturer's instructions. Images were obtained with an Olympus Bx41 microscope, objective UPlanFI 10×/030 and 20×/0.50 ∞/0.17, with an adaptor U-TV0.5xC and a digital camera Q-imaging Micropublisher 5.0 RTV. Images were captured with Q-Capture software (version 3.1) and were imported into Adobe Photoshop 7.0.

DNA sequencing. Genomic DNA was submitted to Otogenetics for whole-exome capture (Agilent V4 (51 Mbp)) and next-generation sequencing on an Illumina HiSeq2000. Next-generation sequencing results were confirmed by Sanger sequencing. *PIK3CD* coding exons were amplified by PCR with exon-specific oligonucleotide primers and GoTaq Hot Start Polymerase (Promega); primer sequences and cycling conditions, **Supplementary Table 2**. Purified PCR products were directly sequenced with BigDye Terminators (version 1.1) and were analyzed on a 3130xL Genetic Analyzer (Applied Biosystems).

Bioinformatics. The DNAnexus interface was used for alignment of the Illumina 'reads' to the hg19 human reference genome and for discovery and genotyping of single-nucleotide polymorphisms and insertions or deletions. To prioritize variant calls, we implemented the ANNOVAR functional annotation package, filtering the output by gene–amino acid annotation, functional prediction scores, nucleotide conservation scores and allele frequencies according to the NCBI dbSNP database (build 137), The 1000 Genomes Project (2012 April release) and the NHLBI GO Exome Sequencing Project (ESP6500). Only nonsynonymous novel variants or variants with population frequencies less than 1% were considered further. All candidates were predicted to be damaging by the SIFT, PP2, LRT, MutationTaster and MutationAssessor tools. Exomic variants were finally prioritized by clinical correlation and analysis of protein structure.

Protein-structure analysis. The Clustal Omega program[49] was used for multiple protein-sequence alignment of p110δ catalytic subunits. As no experimentally derived structural data for p110δ have been reported, we mapped the corresponding positions of the patients' p110δ substitutions onto the structural homolog human p110α (Protein Data Bank accession code, 3HHM). Because of the high sequence homology between p110δ and p110α (39% amino acid identity and 72% amino acid identity and similarity; **Supplementary Fig. 3**), the positions of substitutions in p110δ could be confidently determined on the p110α structure. The reference structure 3HHM contains both the p110α catalytic subunit and the p85α regulatory component of the PI(3)K complex, which allowed comparison the position of the substitutions relative to those of critical membrane contacts that arise from recruitment by p85α.

Cell culture and transfection. Human PBMCs were isolated by density-gradient centrifugation with Ficoll-Paque PLUS (GE Healthcare), washed twice in phosphate buffered saline (PBS) and resuspended at a density of 1×10^6 cells per ml in complete RPMI-1640 medium (Lonza) containing 10% FBS (FBS), 2 mM glutamine, and penicillin and streptomycin (100 U/ml each; Invitrogen). Cells were activated with 1 μg/ml anti-CD3 (HIT3α; BD Biosciences) and 1 μg/ml anti-CD28 (CD28.2; BD Biosciences) in the presence of 100 IU/ml human IL-2. After 3 d, activated T cells were washed and then cultured in complete RPMI-1640 medium supplemented with 100 IU/ml recombinant human IL-2 (R&D Systems). Activated T cell subsets were separated through the use of microbeads coated with anti-CD4 or anti-CD8 (Miltenyi Biotech). The mouse mastocytoma cell line P815 (American Type Culture Collection) and the human H9 T cell line (American Type Culture Collection) were maintained in complete RPMI-1640 medium. Transfection was done with Amaxa Nucleofection kits (Lonza) for primary cells and with standard electroporation for cell lines. For analyses of cytotoxic T lymphocytes (**Fig. 3** and **Supplementary Fig. 5**), human PBMCs were stimulated with irradiated allogeneic buffy coats in the presence of 1 μg/ml phytohemagglutinin and cultured in complete RPMI-1640 medium containing 5% human AB serum (Sigma), 2 mM L-glutamine, 1 mM sodium pyruvate, 1 mM sodium bicarbonate, 50 μM β-mercaptoethanol, 100 U/ml penicillin, 100 μg/ml streptomycin and 100 U/ml recombinant human IL-2.

Flow cytometry. For standard surface staining, PBMCs (1×10^6 cells per sample), sorted cells, expanded T cell populations or cell lines were washed with PBS and incubated for 30 min at 4 °C (in the dark) in 100 μl 5% FBS in PBS with the appropriate fluorochrome-labeled monoclonal antibodies or their isotype-matched control antibodies. After being washed twice with PBS, 1×10^4 to 5×10^4 live cells were analyzed by flow cytometry. The following validated antibodies were used for flow cytometry: anti-CD20 (2H7; BioLegend); anti-CD27 (M-T271), anti-CD10 (HI10A), anti-CD5 (L17F12), anti-IgG (G18-145), anti-CD8 (RPA-T8), anti-IgA (G20-359), anti-CD62L (SK11), anti-interferon-γ (B27), anti-T-bet (O4-46), anti-granzyme B (GB11), anti-LAMP-1 (H4A3), anti-CD38 (HB7) and anti-PD-1 (MIH4; all from BD Biosciences); anti-CD3 (HIT3α (BioLegend) or UCHT1 (BD Biosciences)), anti-CD4 (RPA-T4; BD Biosciences or BioLegend); anti-CCR7 (150503 (R&D Systems) or G043H7 (BioLegend)); anti-CD45RA (H100; eBioscience or BioLegend); and anti-CD57 (TB01; eBioscience). For Phosflow staining, unless otherwise indicated, cells were kept in complete RPMI-1640 medium while alive, then were fixed directly in complete RPMI-1640 medium with BD Lyse-Fix and then permeabilized with Perm Buffer III according to manufacturer's instructions (BD). For Phosflow analyses, the following antibodies were used: Alexa Fluor 647–conjugated antibody to Akt phosphorylated at Ser473 (D9E; Cell Signaling), Alexa Fluor 488–conjugated antibody to Akt phosphorylated at Thr308 (C31E5E; Cell Signaling), phycoerythrin-conjugated antibody to S6 phosphorylated at Ser235 and Ser236 (N7-548; BD Biosciences) and Alexa Fluor 647–conjugated antibody to S6 phosphorylated at Ser240 and Ser244 (D68F8; Cell Signaling).

Tetramer staining. As described before[50], major histocompatibility complex class I tetramers were from Immudex or Proimmune. The CMV epitopes used were the HLA-A*0201–restricted peptides NLVPMVATV from pp65 (UL83) and VTEHDTLLY from pp50 (UL44). The EBV epitopes used were the HLA-A*0201-restricted GLCTLVAML from the lytic antigen BMLF-1 and CLGGLLTMV from latent antigen LMP2, and the HLA-B*0801–restricted peptides RAKFKQLL from BZLF1 lytic protein and FLRGRAYGL from latent protein EBNA3A.

Proliferation assays. For analysis of CFSE dilution, PBMCs (freshly isolated or thawed from samples stored in liquid nitrogen) were incubated with components of the CellTrace CFSE Cell Proliferation Kit (1 μM; Invitrogen). After 5 min, cells were washed twice with complete RPMI-1640 medium. A total of 1×10^5 cells were seeded into 96-well plates, and were stimulated for 72 h with anti-CD3 and anti-CD28 (Dynabeads T-cell activator from Invitrogen) or phytohemagglutinin (1 μg/ml; Sigma-Aldrich) with or without IL-2 (100 IU/ml). Then, cells were stained for 30 min at 4 °C (in the dark) with allophyconcyanin–anti-CD4 (RPA-T4; BD Biosciences or BioLegend) and peridinin chlorophyll protein–anti-CD8 (RPA-T8; BD Biosciences) and washed twice with PBS, and then 1×10^4 live cells were analyzed by flow cytometry (FACSCanto II; Becton Dickinson). Thymidine incorporation was assessed either 3 d (mitogens) or 6 d (antigens) after stimulation in accordance with established guidelines.

Cytokine measurements. PBMCs (1×10^6 per ml) were stimulated for 24–72 h with anti-CD3 and anti-CD28 (Dynabeads T cell activator). Cell-free supernatants were harvested and cytokines were measured simultaneously with Fluorokine MAP Human Base Kit A (R&D Systems) and the Luminex 200 System (Luminex). For intracellular staining of interferon-γ, activated T cells were restimulated for 6 h with plate-bound anti-CD3 (1 μg/ml; OKT3; BD Biosciences)

doi:10.1038/ni.2271

or PMA (phorbol 12-myristate 13-acetate) plus ionomycin in the presence of monensin. Cells were then washed in medium, fixed and permeabilized using BD Cytofix/Cytoperm Buffer and stained intracellularly with anti-interferon-γ (B27; BD Biosciences).

B cell studies. Human B cell subsets were phenotyped by flow cytometry, and naive and memory B cells were sorted and cultured *in vitro* for analysis of proliferation, class switching to IgG, induction of *AICDA* expression and immunoglobulin secretion as described[51].

Immunoblot analysis. Cells were washed in PBS or RPMI medium with no FCS and were immediately lysed in 1% Triton X-100, 50 mM Tris-HCl pH 8, 150 mM NaCl, 2 mM EDTA, 10% glycerol, complete protease inhibitor 'cocktail' (Roche) and phosphatase inhibitor 'cocktails' (Sigma). Proteins were quantified by BCA assay (Pierce). Lysates were then clarified by centrifugation at 15,000*g* at 4 °C for 10 min. Supernatants were transferred to a separate tube and used for subsequent experimentation. Approximately 20 μg total protein was separated by SDS-PAGE and transferred to a nitrocellulose membrane (Bio-Rad). Nonspecific binding in membranes was blocked for 1 h at 21 °C with 5% nonfat dry milk in Tris-buffered saline (TBS), pH 8.5, with 0.01% Tween-20 (TBST), followed by incubation overnight at 4 °C with primary antibody. After membranes were washed for 1 h at 21 °C with TBST, horseradish peroxidase–conjugated secondary antibody was added for an additional hour at 21 °C. The following validated antibodies were used: anti-p110δ (04-401; Millipore), antibody to Akt phosphorylated at Ser473 (4060; Cell Signaling), anti-Akt (4691; Cell Signaling), anti-β-tubulin (2128; Cell Signaling), anti-Flag (M2; Sigma), PTEN (Cell Signaling 9188), PKC-θ (sc-212; Santa Cruz), antibody to phosphorylated Erk (4370; Cell Signaling), anti-Erk (4695; Cell Signaling), ARF6 (5740; Cell Signaling) anti-$p27^{Kip1}$ (3686; Cell Signaling), goat anti–rabbit IgG (4050; Southern Biotech) and goat anti–mouse IgG (1030; Southern Biotech). After a final wash step for 1 h, horseradish peroxidase substrate (Luminata Forte; Millipore) was added to the membranes, which were then subjected to chemiluminscence imaging. Band intensities were quantified with ImageJ software.

Degranulation and cytolysis assays. Activated T cells were stimulated for 2 h or 4 h at 37 °C with plate-bound anti-CD3 (1 μg/ml; HIT3α; BD Biosciences), with nonspecific binding previously blocked with 10% FBS, in the presence of phycoerythrin-conjugated anti-LAMP-1 (H4A3; BD Biosciences). Cells were then washed and stained for surface expression of LAMP-1 and analyzed by flow cytometry. For analysis of general cytolytic activity, P815 cells presenting anti-CD3 were used as targets in a redirected cytotoxicity assay. Cytolytic activity was assayed *in vitro* by measurement of the release of lactate dehydrogenase from target cells with the Cytotox96 cytotoxicity assay according to the manufacturer's instructions (Promega).

Calcium flux assessment. Activated T cell blasts were loaded for 15 min at 37 °C with 1 μM Fluo-4 and 2 μM Fura Red (Molecular Probes) in Powerload (Molecular Probes) before being washed with PBS and resuspended in Hank's balanced-salt solution buffer containing 1.5 mM $CaCl_2$ and 1.5 mM $MgCl_2$. Flux was assessed by flow cytometry upon stimulation with anti-CD3 (HIT3α; BD Biosciences) plus protein A (Sigma).

Confocal imaging. Cells were stimulated with anti-CD3 (HIT3α; BD Biosciences), dropped on poly-L-lysine-coated slides (Electron Microscopy Sciences) and fixed with 3% paraformaldehyde in PBS before being permeabilized for 3–5 min at 21 °C with 0.05% Triton X-100 and blockade of nonspecific binding with 0.5% BSA in PBS. Samples were stained and washed with 0.5% BSA in PBS with anti-p65 (sc-372; Santa Cruz). Slides were mounted with Fluoromount-G with DAPI (4′,6-diamidino-2-phenylindole, dihydrochloride; Southern Biotech) and were visualized with a Leica SP5 confocal microscope (Carl Zeiss) with a 63× objective, and micrographs were analyzed with Imaris 7.4.2 software (Bitplane Scientific).

Glucose uptake. Cells were starved of glucose by incubation for 1 h in PBS before incubation for 10 min or 20 min with 100 μg/ml 2-NBDG (2-deoxy-2-[(7-nitro-2,1,3-benzoxadiazol-4-yl)amino]-D-glucose; Cayman Chemical). Uptake was measured by flow cytometry of signal in the fluorescein channel, collected in log mode (**Fig. 4f**) or linear mode (**Supplementary Fig. 8c**).

Statistical analysis. Data were analyzed with Student's *t*-test (paired or unpaired, with Welch's correction when the standard deviation in the groups was unequal) or a nonparametric Mann-Whitney U-test (when data did not follow a normal distribution) with Prism software (Graph Pad). Only values more than two standard deviations from the mean were excluded from analysis. Whenever possible, at least three patients and three healthy control subjects were examined for each analysis to provide sufficient statistical power.

49. Sievers, F. *et al.* Fast, scalable generation of high-quality protein multiple sequence alignments using Clustal Omega. *Mol. Syst. Biol.* **7**, 539 (2011).
50. Palendira, U. *et al.* Molecular pathogenesis of EBV susceptibility in XLP as revealed by analysis of female carriers with heterozygous expression of SAP. *PLoS Biol.* **9**, e1001187 (2011).
51. Avery, D.T. *et al.* B cell-intrinsic signaling through IL-21 receptor and STAT3 is required for establishing long-lived antibody responses in humans. *J. Exp. Med.* **207**, 155–171 (2010).

doi:10.1038/ni.2271